sequences in order to identify intermediate sequences related to mature neutralizing antibodies. We therefore used well-established maximum likelihood phylogenetic algorithms to analyze antibody sequence data and to build rooted trees of antibody sequences that are derived from a common ancestor (i.e., same VH-germline gene).
38. Several of the non-neutralizing heavy-chain sequences shown in the CDR H3 distribution of Fig. 6 are likely the result of PCR template switching. The single heavy chain depicted in the CDR H3 class 1 contour plot contains a unique CDR H3 sequence (fig. S15a), but with a V gene that displays high similarity to class 3 sequences (table S23). The same observation occurs for the two sequences in the class 2 contour plot. Also, the highly divergent (and outlier) sequence on the CDR H3 class 9 distribution plot contains the same CDR H3 as the other 140 class 9 sequences, but with a V gene that closely matches sequences found in class 8 (table S23b). Because only a few of more than 1500 unique sequences identified by CDR H3 analysis showed dissimilar V genes, and all of these appeared as single or double outliers, template switching can occur but appears to be rare. This rarity is also suggested by an analysis of 606,047 non-IGHV1-2*02 from donor 74 for sequences with the CDR H3s identified in Fig. 6B, which finds less than 100 sequences, of which the majority corresponds to the likely misassigned cluster in the non-IGHV1-2*02 sequence of donor 74 in Fig. 4, as described in (*44*).
39. A similar accumulation of somatic mutations was shown (*45*) with the broadly neutralizing antibodies PG9 and PG16 to correlate with an increase in neutralization breadth and potency.
40. D. Nemazee, M. Weigert, *J. Exp. Med.* **191**, 1813 (2000).
41. E. Edry, D. Melamed, *J. Immunol.* **173**, 4265 (2004).
42. J. Glanville *et al.*, *Proc. Natl. Acad. Sci. U.S.A.* **106**, 20216 (2009).
43. H. Zhou, Y. Zhou, *Protein Sci.* **11**, 2714 (2002).
44. The peak at ~25% IGHV1-2*02 divergence and 88% identity was also seen in the sequence plot for sequences of non-IGHV1-2*02 origin. Cross-donor and CDR H3 analyses shows that these putative non-IGHV1-2*02–derived sequences segregate with VRC01-like antibodies in dendrograms and have CDR H3s that are identical to confirmed VRC01-like antibodies (fig. S16), indicating that sequences in the non-IGHV1-2*02 cluster are likely misassigned and actually of IGHV1-2*02 origin.
45. M. Pancera *et al.*, *J. Virol.* **84**, 8098 (2010).
46. E. A. Kabat, T. T. Wu, K. S. Gottesman, C. Foeller, *Sequences of Proteins of Immunological Interest, 5th Edition* (U.S. Department of Health and Human Services, Washington, DC, 1991).
47. E. Krissinel, K. Henrick, *J. Mol. Biol.* **372**, 774 (2007).

Acknowledgments: X.W., T.Z., J. Z., G.J.N., M.R., L.S., P.D.K., and J.R.M. designed research; B.Z., C.W., X.C., M.L., K.M., S.O.D., S.P., S.D.S., W.S., L.W., Y.Y., Z.Y.Y., Z.Y., NISC, and J.M. performed experiments; X.W. isolated and characterized VRC01-like antibodies by RSC3 probe, devised and prepared samples for 454 pyrosequencing, and assisted with functional characterization; T.Z. determined and analyzed structures of VRC-PG04 and VRC03 with gp120 and assisted with functional characterization; J.Z. devised and carried out computational bioinformatics on the antibodyome; M.B., J.A.C, S.H.K, N.E.S., and B.F.H. contributed donor 0219 materials; M.S., D.R.B., and W.C.K contributed Protocol G materials, including donor 74; N.D.R. and M.C. contributed donor 45 materials; X.W., T.Z., J.Z, I.G., N.S.L., Z.Z., L.S., P.D.K., and J.R.M. analyzed the data; and L.S., G.J.N., P.D.K., and J.R.M. wrote the paper, on which all authors commented. We thank J. Almeida and D. Douek for protocols of PBMC cDNA preparation and for helpful discussions; J. Stuckey for assistance with figures; T. Wrin for sequence information on the donor 74 virus; J. Binley, D. Montefiori, L. Morris, and G. Tomaras for donor 0219 serum characterization; and all of the IAVI Protocol G team members and the Protocol G clinical investigators, specifically, G. Miiro, A. Pozniak, D. McPhee, O. Manigart, E. Karita, A. Inwoley, W. Jaoko, J. DeHovitz, L.-G. Bekker, P. Pitisuttithum, R. Paris, J. Serwanga, and S. Allen. We also thank H. Sato, I. Wilson, and members of the Structural Biology Section and Structural Bioinformatics Core, Vaccine Research Center, for discussions or comments on the manuscript. Support for this work was provided by the Intramural Research Program of the Vaccine Research Center, National Institute of Allergy and Infectious Diseases, and the National Human Genome Research Institute, NIH; by grants from the International AIDS Vaccine Initiative's Neutralizing Antibody Consortium; and by the Center for HIV AIDS Vaccine Immunology grant AI 5U19 AI 067854-06 from NIH. Use of sector 22 (Southeast Region Collaborative Access Team) at the Advanced Photon Source was supported by the U.S. Department of Energy, Basic Energy Sciences, Office of Science, under contract W-31-109-Eng-38. Structure factors and coordinates for antibodies VRC03 and VRC-PG04 in complex with HIV-1 gp120 have been deposited with the Protein Data Bank under accession codes 3SE8 and 3SE9, respectively. We have also deposited deep sequencing data for donors 45 and 74 (Appendices 1 to 4) used in this study to National Center for Biotechnology Information Short Reads Archives (SRA) under accession no. SRP006992. Information deposited with GenBank includes the heavy- and light-chain variable region sequences of probe-identified antibodies VRC-PG04 and VRC-PG04b (accession nos. JN159464 to JN159467), VRC-CH30, VRC-CH31, and VRC-CH32 (JN159434 to JN159439), and VRC-CH33 and VRC-CH34 (JN159470 to 159473), as well as the sequences of genomically identified neutralizers: 24 heavy chains from donor 74, 2008 (JN159440 to JN159463), two heavy chains from donor 45, 2008 (JN159474 and JN159475), two light chains from donor 45, 2001 (JN159468 and JN159469), and 1561 unique sequences associated with neutralizing CDR H3 distributions with at least one low divergent member shown in Fig. 6B and fig. S16 (JN157873 to JN159433).

Supporting Online Material
www.sciencemag.org/cgi/content/full/science.1207532/DC1
Materials and Methods
Figs. S1 to S20
Tables S1 to S23
References (*48*–*82*)
Appendices 1 to 4

26 April 2011; accepted 15 July 2011
Published online 11 August 2011;
10.1126/science.1207532

Kepler-16: A Transiting Circumbinary Planet

Laurance R. Doyle,[1]* Joshua A. Carter,[2] Daniel C. Fabrycky,[3] Robert W. Slawson,[1] Steve B. Howell,[4] Joshua N. Winn,[5] Jerome A. Orosz,[6] Andrej Prša,[7] William F. Welsh,[6] Samuel N. Quinn,[8] David Latham,[8] Guillermo Torres,[8] Lars A. Buchhave,[9,19] Geoffrey W. Marcy,[11] Jonathan J. Fortney,[12] Avi Shporer,[13,14] Eric B. Ford,[15] Jack J. Lissauer,[4] Darin Ragozzine,[2] Michael Rucker,[16] Natalie Batalha,[16] Jon M. Jenkins,[1] William J. Borucki,[4] David Koch,[4] Christopher K. Middour,[17] Jennifer R. Hall,[17] Sean McCauliff,[17] Michael N. Fanelli,[18] Elisa V. Quintana,[1] Matthew J. Holman,[8] Douglas A. Caldwell,[1] Martin Still,[18] Robert P. Stefanik,[8] Warren R. Brown,[8] Gilbert A. Esquerdo,[8] Sumin Tang,[8] Gabor Furesz,[8,10] John C. Geary,[8] Perry Berlind,[20] Michael L. Calkins,[20] Donald R. Short,[21] Jason H. Steffen,[22] Dimitar Sasselov,[8] Edward W. Dunham,[23] William D. Cochran,[24] Alan Boss,[25] Michael R. Haas,[4] Derek Buzasi,[26] Debra Fischer[27]

We report the detection of a planet whose orbit surrounds a pair of low-mass stars. Data from the Kepler spacecraft reveal transits of the planet across both stars, in addition to the mutual eclipses of the stars, giving precise constraints on the absolute dimensions of all three bodies. The planet is comparable to Saturn in mass and size and is on a nearly circular 229-day orbit around its two parent stars. The eclipsing stars are 20 and 69% as massive as the Sun and have an eccentric 41-day orbit. The motions of all three bodies are confined to within 0.5° of a single plane, suggesting that the planet formed within a circumbinary disk.

A planet with two suns is a familiar concept from science fiction. However, the evidence for the existence of circumbinary planets—those that orbit around both members of a stellar binary—has been limited. A few good cases have been made for circumbinary planets based on the timing of stellar eclipses [see, e.g., (*1*–*3*)], but in no previous case have astronomers obtained direct evidence of a circumbinary planet by observing a planetary transit (a miniature eclipse as the planet passes directly in front of a star). Detection of a transit greatly enhances confidence in the reality of the planet and provides unusually precise knowledge of its mass, radius, and orbital parameters (*4*).

Here we present the detection of a transiting circumbinary planet around a binary star system based on photometric data from the NASA Kepler spacecraft. Kepler is a 0.95-m space telescope that monitors the optical brightness of about 155,000 stars within a field encompassing 105 square degrees in the constellations Cygnus and Lyra (*5*–*8*).

Star number 12644769 from the Kepler Input Catalog was identified as an eclipsing binary with a 41-day period, from the detection of its mutual eclipses (*9*). Eclipses occur because the orbital plane of the stars is oriented nearly edge-on as viewed from Earth. During primary eclipses, the larger star, denoted "A," is partially eclipsed by the smaller star "B," and the system flux declines by about 13%. During secondary eclipses, B is completely occulted by A, and the resulting drop in flux is only about 1.6% because B is rel-

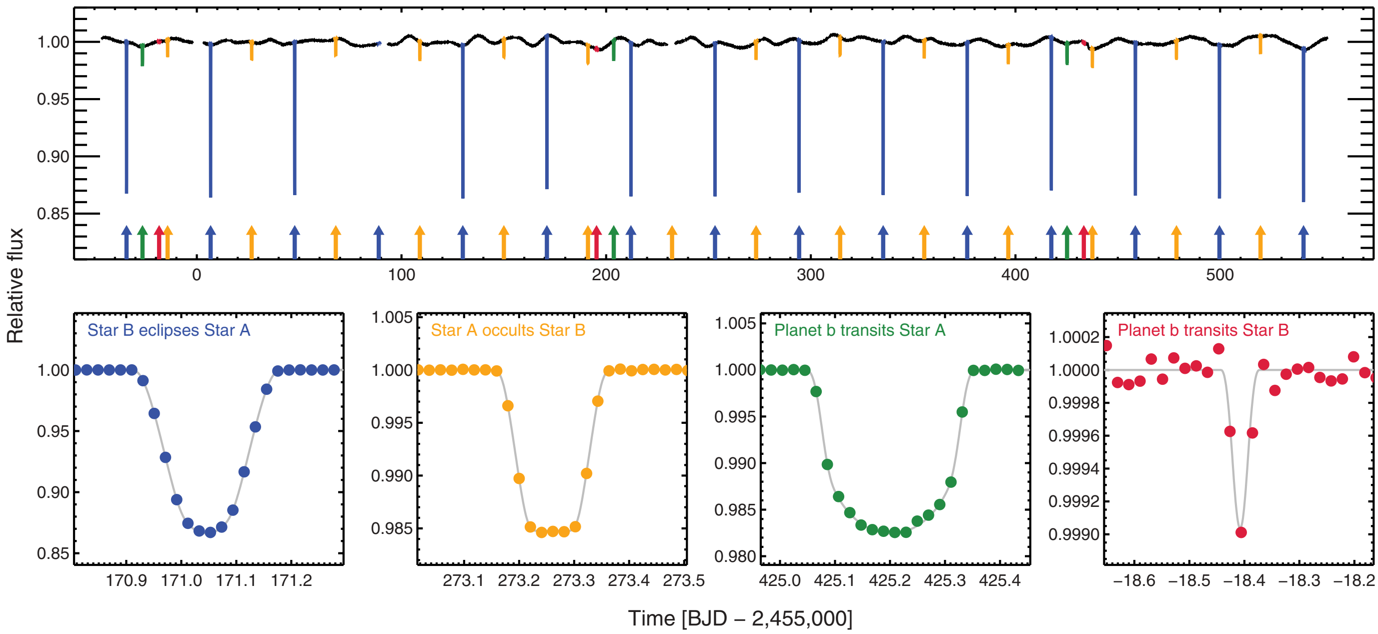

Fig. 1. Photometry of Kepler-16. (**Top**) Photometric time series from the Kepler spacecraft of star system Kepler-16 (KIC 12644769, KOI-1611, 2MASS 19161817+5145267, Kepler magnitude = 11.762). Each data point is the relative brightness at a given time [in barycentric Julian days (BJDs)]. The 1% variations on ~10-day time scales are probably due to starspots carried around by stellar rotation (a periodogram gives a rotation period of about 35 days). The sharp dips are eclipses, appearing as vertical lines in this 600-day plot. They are identified as primary (B eclipses A, blue), secondary (A occults B, yellow), tertiary (b transits A, green), and quaternary (b transits B, red). Because of interruptions in Kepler observing, data are missing from one primary eclipse at BJD 2,455,089, and one secondary eclipse at BJD 2,455,232. Note in particular the shifting order of the tertiary (green) and quaternary (red) eclipses: The first and third pairs begin with the tertiary eclipse, whereas the second pair leads with the quaternary eclipse. This is because the stars' orbital motion places them in different positions at each inferior conjunction of the planet. The stars silhouette the planet as they move behind it. (**Bottom**) Closeups (narrower scales in time and relative flux) of representative examples of each type of eclipse, along with the best-fitting model (gray), with parameters from Table 1.

atively small and has a lower surface brightness (Fig. 1).

This target drew further attention when three additional drops in brightness were detected outside of the primary and secondary eclipses, separated by intervals of 230.3 and 221.5 days (*10*). These tertiary eclipses could not be attributed to the stars alone, and indicated the presence of a third body. The differing intervals between the tertiary eclipses are simply explained if the third body is in a circumbinary orbit, because stars A and B would be in different positions in their mutual orbit each time the third body moved in front of them (*11*, *12*). In contrast, there would be no ready explanation for the shifting times of the tertiary eclipses if they were produced by a background star system or some other unrelated event.

During tertiary eclipses, the total light declines by 1.7%. Because this is larger than the 1.6% decline during secondary eclipses (when star B is completely concealed), the tertiary eclipses had to be transits of the third body across star A. This interpretation was supported by the subsequent detection of weaker 0.1% quaternary eclipses, which were consistent with the passage of the third body across star B. The observed time of this quaternary eclipse was used to predict two other times of quaternary eclipses that should have been present in the data, and these two events were subsequently detected (Fig. 1).

Because the third body covers only 1.7% of the area of star A, which was determined to be smaller than the Sun on the basis of its broadband colors (*10*), the circumbinary body was suspected to be either a planet or a third star with grazing eclipses. Decisive evidence that it is a planet came from investigation of the timing of the stellar eclipses. The primary and secondary eclipse times were found to depart from strict periodicity by deviations on the order of 1 min. A third body causes timing variations in two ways. First, there is a light travel-time effect: The third body induces a periodic motion of the center of mass of the stellar binary, causing periodic variations in the time required for the eclipse signals to reach Earth (*13*, *14*). Second, there is a dynamical effect: The gravitational attraction of each star to the third body varies with time because of the changing positions of all three bodies, causing perturbations in the stars' orbital parameters and therefore in the eclipse times (*15*, *16*). Both effects

[1]Carl Sagan Center for the Study of Life in the Universe, SETI Institute, 189 Bernardo Avenue, Mountain View, CA 94043, USA. [2]Hubble Fellow, Harvard-Smithsonian Center for Astrophysics, 60 Garden Street, Cambridge, MA 02138, USA. [3]Hubble Fellow, Department of Astronomy and Astrophysics, University of California, Santa Cruz, CA 95064, USA. [4]NASA Ames Research Center, Moffett Field, CA 94035, USA. [5]Department of Physics and Kavli Institute for Astrophysics and Space Research, Massachusetts Institute of Technology, 77 Massachusetts Avenue, Cambridge, MA 02139, USA. [6]Department of Astronomy, San Diego State University, 5500 Campanile Drive, San Diego, CA 92182–1221, USA. [7]Department of Astronomy and Astrophysics, Villanova University, 800 East Lancaster Avenue, Villanova, PA 19085, USA. [8]Harvard-Smithsonian Center for Astrophysics, 60 Garden Street, Cambridge, MA 02138, USA. [9]Niels Bohr Institute, University of Copenhagen, DK-2100 Copenhagen, Denmark. [10]Centre for Star and Planet Formation, Natural History Museum of Denmark, University of Copenhagen, DK-1350 Copenhagen, Denmark. [11]Department of Astronomy, University of California, Berkeley, CA 94720, USA. [12]Department of Astronomy and Astrophysics, University of California, Santa Cruz, Santa Cruz, CA 95064, USA. [13]Las Cumbres Observatory Global Telescope Network, 6740 Cortona Drive, Suite 102, Santa Barbara, CA 93117, USA. [14]Department of Physics, Broida Hall, University of California, Santa Barbara, CA 93106, USA. [15]211 Bryant Space Science Center, Gainesville, FL 32611–2055, USA. [16]Department of Physics, San Jose State University, San Jose, CA 95192, USA. [17]Orbital Sciences Corporation/NASA Ames Research Center, Moffett Field, CA 94035, USA. [18]Bay Area Environmental Research Institute/NASA Ames Research Center, Moffett Field, CA 94035, USA. [19]Konkoly Observatory, Konkoly ut 15-17, Budapest, H-1121, Hungary. [20]Fred Lawrence Whipple Observatory, Smithsonian Astrophysical Observatory, Amado, AZ 85645, USA. [21]Department of Mathematics, San Diego State University, 5500 Campanile Drive, San Diego, CA 92182, USA. [22]Fermilab Center for Particle Astrophysics, Post Office Box 500, Batavia, IL 60510, USA. [23]Lowell Observatory, Flagstaff, AZ 86001, USA. [24]McDonald Observatory, University of Texas at Austin, Austin, TX 78712, USA. [25]Carnegie Institute of Washington, Washington, DC 20015, USA. [26]Eureka Scientific, 2452 Delmer Street, Suite 100, Oakland, CA 94602, USA. [27]Department of Astronomy, Yale University, New Haven, CT 06511, USA.

*To whom correspondence should be addressed. E-mail: ldoyle@seti.org

depend on the mass of the third body. Therefore, we could constrain the mass of the third body by fitting the eclipse data with a numerical model of three-body gravitational interactions. This model, described below in detail, showed that the third body must be less massive than Jupiter.

Hence, based on the depth of the tertiary eclipses and on the magnitude of the eclipse timing variations, the third body was shown to be a transiting circumbinary planet. The model was based on the premise that the three bodies move under the influence of mutual Newtonian gravitational forces. For this purpose, we modified the computer code that was used to model the triple star system KOI-126 (*17*) [supporting online material (SOM)]. The leading-order relativistic correction to the force law was included, although it proved to be unimportant. The bodies' positions were calculated with a Bulirsch-Stoer algorithm and corrected for the finite propagation speed of light across the system before being compared to the data. The loss of light due to eclipses was calculated by assuming the disks of stars A and B to be circular, with a quadratic law describing the decline in intensity toward the limb (*18*). We also allowed for an additional time-independent source of light to account for any possible background stars within the Kepler photometric aperture. In practice, this parameter was found to be consistent with zero and bounded to be less than 1.3% of the total light of the system (*19*).

We fitted all of the photometric data within 6 hours of any eclipse or transit. Before fitting, a linear trend was removed from each segment, to correct for the slow starspot-induced variations evident in Fig. 1. A successful model had to be

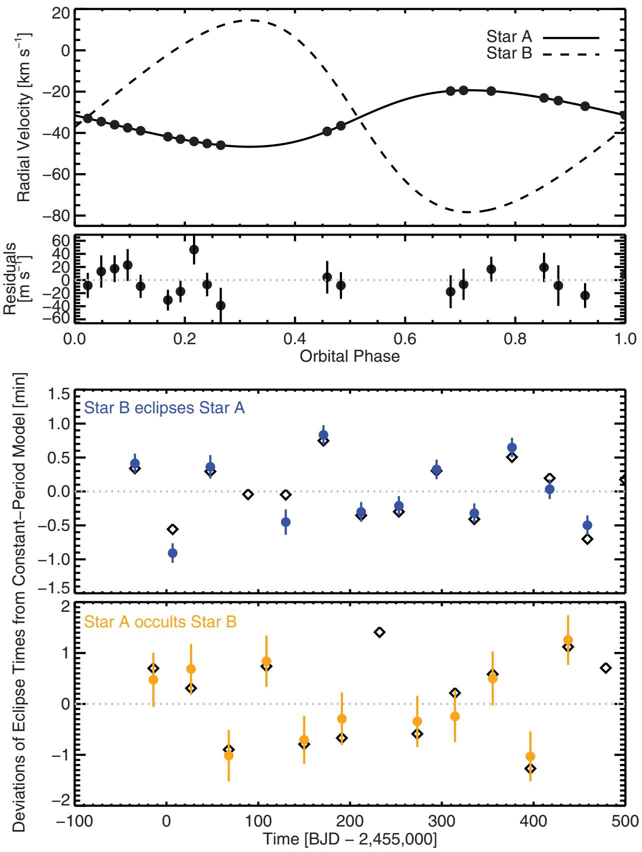

Fig. 2. Radial-velocity variations and perturbations of eclipse times. (**Top**) Observed radial-velocity variations of star A as a function of orbital phase, based on observations with the spectrograph of the Tillinghast 1.5-m telescope at the Fred Lawrence Whipple Observatory on Mount Hopkins, Arizona (SOM). Solid dots are the data, and the smooth curve is the best-fitting model. Although only the light from star A could be detected in the spectra, the model for star B's motion is also shown. Residuals from the best model fits are given just below the radial velocity curve. (**Middle** and **Bottom**) Deviations of the stellar eclipse times from strict periodicity, as observed (colored dots) and modeled (open diamonds). As noted previously, one primary eclipse and one secondary eclipse were missed. The deviations are on the order of 1 min for both primary and secondary stellar eclipses. In the model, the effects of dynamical perturbations are dominant, with light-time variations contributing only at the level of 1 s. If the third body were more massive than a planet (>13 jovian masses), the timing variations would have exceeded 30 min. This would have been off the scale of the diagram shown here, and in contradiction with the observations.

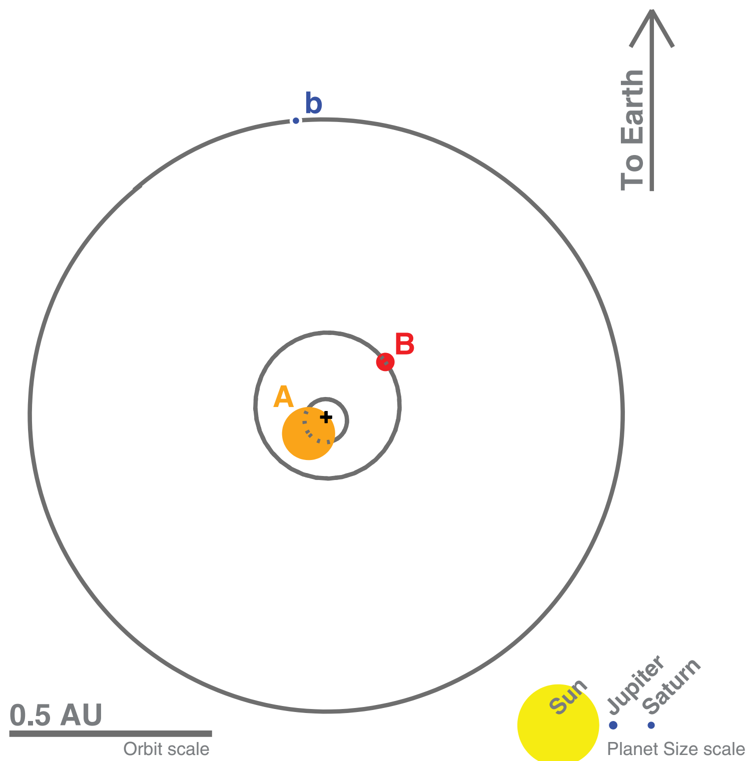

Fig. 3. Scale diagram of the Kepler-16 system. The current orbits of the Kepler-16 system are shown as gray curves. The sizes of the bodies (including the Sun, Jupiter, and Saturn) are in the correct proportions to one another, but they are on a scale 20 times larger than the orbital distance scale. The binary and circumbinary planet orbital planes lie within 0.4° of each other (Table 1), so the orbits are essentially flat, as drawn. The planet's orbital eccentricity is nearly zero, whereas the orbital eccentricity of the binary star system is presently about 0.16. A "+" symbol marks the center of mass of all three bodies.

compatible with the timings, durations, and depths of the primary and secondary stellar eclipses, as well as the transits of the planet across both stars. The model also had to account for the slight departures from strict periodicity of the stellar eclipses. Furthermore, to pin down the stellar masses and provide an absolute distance scale, we undertook spectroscopic observations to track the radial velocity variations of star A (Fig. 2, top panel).

The model parameters were adjusted to fit the photometric and radial-velocity data (Table 1). Figures 1 and 2 show the very good match that was achieved between the model and the data. Uncertainties in the parameters were determined with a Differential Evolution Markov Chain Monte Carlo simulation (*20*) (SOM).

Due to the presence of three-body effects (namely, the shifts in eclipse times and transit durations), the masses, radii, and orbital distances of this system are well determined in absolute units, not just in relative units. The eclipse timing variations are dominated by the effects of dynamical perturbations, with light-time variations contributing only at the level of 1 s. The third body's dimensions are well within the planetary regime, with a mass of 0.333 ± 0.016 and a radius of 0.7538 ± 0.0025 those of Jupiter. Following the convention of (*21*), we can denote the third body Kepler-16 (AB)-b, or simply "b" when there is no ambiguity.

Table 1. Characteristics of the Kepler-16 system. For all parameters except T_{eff} and [m/H] (which are described in the SOM), the results are based on the photometric-dynamical model. The quoted values and uncertainty intervals are based on the 15.85, 50, and 84.15% levels of the cumulative distributions of the marginalized posteriors for each parameter, making them analogous to 1σ intervals for Gaussian statistics. The quoted orbital parameters are osculating Jacobian parameters at BJD 2,455,212.12316. The distance from Kepler-16 to Earth has not been measured, but is probably about 200 light years, judging from the apparent brightness of star A and theoretical models of stellar structure that give a crude estimate of its intrinsic luminosity.

Parameter	Value and uncertainty
Star A	
Mass, M_A (M solar)	$0.6897^{+0.0035}_{-0.0034}$
Radius, R_A (R solar)	$0.6489^{+0.0013}_{-0.0013}$
Mean density, ρ_A (g/cm^3)	$3.563^{+0.017}_{-0.016}$
Surface gravity, log g_A (cgs)	$4.6527^{+0.0017}_{-0.0016}$
Effective temperature, T_{eff} (K)	4450 ± 150
Metallicity, [m/H]	–0.3 ± 0.2
Star B	
Mass, M_B (M solar)	$0.20255^{+0.00066}_{-0.00065}$
Radius, R_B (R solar)	$0.22623^{+0.00059}_{-0.00053}$
Mean density, ρ_B (g/cm^3)	$24.69^{+0.13}_{-0.15}$
Surface gravity, log g_B (cgs)	$5.0358^{+0.0014}_{-0.0017}$
Planet b	
Mass, M_b ($M_{Jupiter}$)	$0.333^{+0.016}_{-0.016}$
Radius, R_b ($R_{Jupiter}$)	$0.7538^{+0.0026}_{-0.0023}$
Mean density, ρ_b (g/cm^3)	$0.964^{+0.047}_{-0.046}$
Surface gravity, g_b (m/s^2)	$14.52^{+0.70}_{-0.69}$
Binary star orbit	
Period, P_1 (day)	$41.079220^{+0.000078}_{-0.000077}$
Semi-major axis length, a_1 (AU)	$0.22431^{+0.00035}_{-0.00034}$
Eccentricity, e_1	$0.15944^{+0.00061}_{-0.00062}$
Argument of periapse, ω_1 (deg)	$263.464^{+0.026}_{-0.027}$
Mean longitude, λ_1 (deg)	$92.3520^{+0.0011}_{-0.0011}$
Inclination, i_1 (deg)	$90.3401^{+0.0016}_{-0.0019}$
Longitude of nodes, Ω_1 (deg)	≡0 (by definition)
Circumbinary planet orbit	
Period, P_2 (day)	$228.776^{+0.020}_{-0.037}$
Semi-major axis length, a_2 (AU)	$0.7048^{+0.0011}_{-0.0011}$
Eccentricity, e_2	$0.0069^{+0.0010}_{-0.0015}$
Argument of periapse, ω_2 (deg)	$318^{+10.}_{-22.}$
Mean longitude, λ_2 (deg)	$106.51^{+0.32}_{-0.16}$
Inclination, i_2 (deg)	$90.0322^{+0.0022}_{-0.0023}$
Longitude of nodes, Ω_2 (deg)	$0.003^{+0.013}_{-0.013}$
Other parameters	
Flux ratio of stars in Kepler bandpass, F_B/F_A	$0.01555^{+0.00010}_{-0.00006}$
Upper limit on third light (95% conf.), $F_X/(F_A + F_B)$	<0.013
Radial velocity parameter of barycenter, γ (km s^{-1})	$-32.769^{+0.035}_{-0.035}$
Photometric noise parameter, σ_{phot}	$0.0002403^{+0.0000062}_{-0.0000060}$

Considering its bulk properties, the planet is reminiscent of Saturn but with a higher mean density (0.964 g cm^{-3}, compared to the Saturnian density of 0.687 g cm^{-3}). This suggests a greater degree of enrichment by heavy elements. With a mass and radius, one can begin to model a planet's interior structure, which will depend on age because planets cool and contract with time. Usually the stellar age is used as a proxy for the planetary age, but in this case the stellar age is not unambiguous. The primary star (A) is a slow rotator (with a period of about 35.1 days, judging from the out-of-eclipse variations), which is usually indicative of old age. In contrast, its level of starspot activity and chromospheric emission (Mount Wilson *S* value = 1.10) are indicative of youth. The spectroscopic determination of star A's heavy-element fraction ([m/H] = –0.3 ± 0.2) is also relatively uncertain, making it more difficult to estimate the age with theoretical evolutionary models. Nevertheless, for any age greater than 0.5 billion years, the planet's interior would include 40 to 60 Earth masses of heavy elements, according to standard planetary models (*22*). This would imply a composition of approximately half gas (hydrogen and helium) and half heavy elements (presumably ice and rock). Saturn, in contrast, is at least two-thirds gas by mass (*23*).

To investigate the long-term (secular) changes in the orbital parameters, and to check on the system's stability, we integrated the best-fitting model forward in time by two million years. Within the context of our gravitational three-body model, secular variations occur on a time scale of about 40 years, without any significant excursions in orbital distance that would have led to instability. The planet's orbital eccentricity reaches a maximum of about 0.09. Likewise, the planet's line-of-sight orbital inclination changes by 0.2°, which is large enough that transits are only visible from Earth about 40% of the time (averaged over centuries). In particular, the planetary transits across star A should cease in early 2018, and return sometime around 2042. The planetary transits across star B are already grazing and are predicted to disappear for 35 years beginning in May 2014.

The planet experiences swings in insolation due to the motion of the stars on short time scales and to secular changes in the planet's orbit on long time scales. These variations are likely to affect the temperature and structure of the planet's atmosphere. The planet's current equilibrium temperature, averaged over several orbits, is between 170 and 200 K, assuming isotropic re-radiation of the stellar flux and a Bond albedo between 0.2 and 0.5 (in the neighborhood of Saturn's value of 0.34). The orbital motions of the stars and planet are expected to produce seasonal temperature variations of around 30 K.

The planetary orbit is aligned with the stellar orbit to within 0.4°. This extreme coplanarity suggests that the planet was formed along with the stars, within a circumbinary protoplanetary disk, as opposed to being captured from another system. Planetesimal formation around an eccentric binary is a theoretical challenge, because of the large collision velocities of particles that are stirred by the stellar binary (*24*), although the detection of debris disks around close binaries has been interpreted as dust produced by colliding planetesimals (*25*). Subsequent stages of planet formation around binaries have been studied theoretically, both for terrestrial planets (*26*) and gas giants (*27*), but these and other theoretical studies (*28*) have lacked a well-specified circumbinary planetary system that could allow such a refinement of models.

Finally, the stars themselves are worthy of attention, independently of the planet. It is rare to measure the masses and radii of such small stars with such high precision, using geometrical and dynamical methods independent of stellar evolutionary models. In particular, star B, with only 20% the mass of the Sun, is the smallest main-sequence star for which such precise mass and radius data are available (*29*) (Fig. 3). The mass ratio of 0.29 is also among the smallest known for binaries involving fully convective stars at the low-mass end of the main sequence (*28*). With well-characterized low-mass stars, in addition to a transiting circumbinary planet, this makes Kepler-16 a treasure for both exoplanetary and stellar astrophysical investigations.

References and Notes

1. H.-J. Deeg *et al.*, *Astron. Astrophys.* **480**, 563 (2008).
2. J. W. Lee *et al.*, *Astron. J.* **137**, 3181 (2009).
3. K. Beuermann *et al.*, *Astron. Astrophys.* **521**, L60 (2010).
4. J. N. Winn, in *Exoplanets*, S. Seager, Ed. (Univ. of Arizona Press, Tucson, AZ, 2010), pp. 55–77.
5. W. J. Borucki *et al.*, *Science* **327**, 977 (2010).
6. D. Koch *et al.*, *Astrophys. J. Lett.* **713**, L79 (2010).
7. D. A. Caldwell *et al.*, *Astrophys. J. Lett.* **713**, L92 (2010).
8. J. M. Jenkins *et al.*, *Astrophys. J. Lett.* **713**, L87 (2010).
9. A. Prša *et al.*, *Astron. J.* **141**, 83 (2010).
10. R. W. Slawson *et al.*, Kepler eclipsing binary stars. II. 2166 eclipsing binaries in the second data release; preprint available at http://arxiv.org/abs/1103.1659.
11. H. J. Deeg *et al.*, *Astron. Astrophys.* **338**, 479 (1998).
12. L. R. Doyle *et al.*, *Astrophys. J.* **535**, 338 (2000).
13. J. Irwin, *Astrophys. J.* **116**, 211 (1952).
14. P. Sybilski, M. Konacki, S. Kozlowski, *Mon. Not. R. Astron. Soc.* **405**, 657 (2011).
15. Z. Kopal, *Close Binary Systems* (Chapman & Hall, London, 1959).
16. R. Schwarz, N. Haghighipour, S. Eggl, E. Pilat-Lohinger, B. Funk, *Mon. Not. R. Astron. Soc.* **414**, 2763 (2011).
17. J. A. Carter *et al.*, *Science* **331**, 562 (2011).
18. K. Mandel, E. Agol, *Astrophys. J.* **580**, L171 (2002).
19. Speckle interferometric imaging with the WIYN telescope also restricted any contaminating stars separated by >0.02 arc sec to have a flux less than 3% of the system. For the methodology, see (*30*).
20. C. J. F. Ter Braak, *Stat. Comput.* **16**, 239 (2006).
21. F. V. Hessman *et al.*, "On the naming convention used for multiple star systems and extrasolar planets," open letter to the stellar and exoplanet communities, available at http://arxiv.org/abs/1012.0707.
22. J. J. Fortney, M. S. Marley, J. W. Barnes, *Astrophys. J.* **659**, 1661 (2007).
23. T. Guillot, *Annu. Rev. Earth Planet. Sci.* **33**, 493 (2005).
24. H. Scholl, F. Marzari, P. Thebault, *Mon. Not. R. Astron. Soc.* **380**, 1119 (2007).
25. D. E. Trilling *et al.*, *Astrophys. J.* **658**, 1289 (2007).
26. E. V. Quintana, J. J. Lissauer, *Icarus* **185**, 1 (2006).
27. A. Pierens, R. P. Nelson, *Astron. Astrophys.* **483**, 633 (2008).
28. N. Haghighipour, *Planets in Binary Star Systems* (Astrophysics and Space Science Library, vol. 366, Springer, New York, 2010).
29. G. Torres, J. Andersen, A. Giménez, *Astron. Astrophys. Rev.* **18**, 67 (2010).
30. S. B. Howell, M. E. Everett, W. Sherry, E. Horch, D. Ciardi, *Astron. J.* **142**, 19 (2011).

Acknowledgments: NASA's Science Mission Directorate provided funding for the Kepler Discovery mission. L.R.D. acknowledges the NASA Kepler Participating Scientist Program (grant no. NNX08AR15G) and helpful discussions with the Kepler Science Team. J.A.C. and D.C.F. acknowledge support for this work provided by NASA through Hubble Fellowship grants HF-51267.01-A and HF-51272.01-A awarded by the Space Telescope Science Institute, which is operated by the Association of Universities for Research in Astronomy for NASA, under contract NAS 5-26555. J.N.W. is grateful for support from the NASA Origins program (grant NNX09AB33G). The Kepler data used in this analysis can be downloaded from http://archive.stsci.edu/prepds/kepler_hlsp.

Supporting Online Material

www.sciencemag.org/cgi/content/full/333/6049/1602/DC1
SOM Text
Figs. S1 to S3
Tables S1 to S5
References (*31–41*)

8 July 2011; accepted 18 August 2011
10.1126/science.1210923

REPORTS

Unclicking the Click: Mechanically Facilitated 1,3-Dipolar Cycloreversions

Johnathan N. Brantley, Kelly M. Wiggins, Christopher W. Bielawski*

The specific targeting of covalent bonds in a local, anisotropic fashion using mechanical methods offers useful opportunities to direct chemical reactivity down otherwise prohibitive pathways. Here, we report that embedding the highly inert 1,2,3-triazole moiety (which is often prepared using the canonical "click" coupling of azides and alkynes) within a poly(methyl acrylate) chain renders it susceptible to ultrasound-induced cycloreversion, as confirmed by comprehensive spectroscopic and chemical analyses. Such reactivity offers the opportunity to develop triazoles as mechanically labile protecting groups or for use in readily accessible materials that respond to mechanical force.

The 1,3-dipolar cycloaddition of azide and alkyne moieties (*1*, *2*), which allows access to a variety of substituted triazoles, is included under the umbrella of "click" chemistry. This reaction has found broad applicability over the past decade because it exhibits rapid kinetics under mild conditions, high functional group and solvent tolerance, and good atom economy, and it has a propensity to generate relatively chemically inert and thermally stable products. In addition to finding compelling use in molecular and polymer functionalizations, this coupling motif has been applied to robust, chemically orthogonal ligations for the study of biological systems (*3–11*). However, a consequence of the high kinetic stability of these triazole products is that simple chemical or thermal treatments capable of cleanly reverting the coupling reactions into their constituent azides and alkynes are unknown. We envisioned that mechanical force could be used to surmount the otherwise inaccessible barrier to triazole cycloreversion; that is, under the appropriate mechanical stress, triazoles might not retain their structural integrity. Such a retrocycloaddition would also indicate that triazoles are not necessarily orthogonal to chemical transformations and would provide a method by which reactive azide or alkyne intermediates could be selectively unmasked to effect desired transformations (Scheme 1).

Recent advances in mechanochemistry (*12*)—wherein exogenous forces can be directed to mechanophores, or small molecules possessing mechanically labile bonds, through the judicious attachment of polymer chains—have demonstrated that formally disallowed pericyclic reactions and thermally inaccessible isomerizations can be readily induced through site-specific mechanical activation (*13–18*). Such forces can be harnessed through the application of ultrasound to polymer solutions, whereby cavitation induces velocity gradients and attendant stress to the

Department of Chemistry and Biochemistry, The University of Texas at Austin, 1 University Station A1590, Austin, TX 78712, USA.

*To whom correspondence should be addressed. E-mail: bielawski@cm.utexas.edu